

Understanding the impurity gettering effect of polysilicon/oxide passivating contact structures through experiment and simulation

AnYao Liu^{a,*}, Zhongshu Yang^a, Frank Feldmann^b, Jana-Isabelle Polzin^b, Bernd Steinhauser^b, Sieu Pheng Phang^a, Daniel Macdonald^a

^a School of Engineering, College of Engineering and Computer Science, The Australian National University, Canberra, ACT, 2601, Australia

^b Fraunhofer Institute for Solar Energy Systems ISE, Heidenhofstr. 2, D-79110, Freiburg, Germany



ARTICLE INFO

Keywords:
Gettering
Silicon solar cells
Polysilicon/oxide passivating contacts
Silicon oxide
Diffusion
Iron

ABSTRACT

Polysilicon/oxide (poly-Si/SiO_x) passivating contacts are a promising technology for the next-generation of high-efficiency silicon solar cells. The structure can be realised by a range of fabrication techniques, which can induce very different impurity gettering effects during the formation process. Understanding the different gettering effects will enable tailored solutions to optimise the gettering efficiency in device fabrication. This paper demonstrates a method to separately quantify the impact of each component on the overall gettering effect of the poly-Si/SiO_x passivating contact structures. These components consist of the heavily doped poly-Si layer, in terms of its gettering strength; the SiO_x interlayer, regarding its potential blocking effect for slowing down the diffusion of impurities; and the dopant in-diffused surface regions of the silicon wafer bulk directly below the SiO_x interlayer, which may have a small additional gettering effect due to heavy doping. Phosphorus in-situ doped poly-Si layers from plasma-enhanced chemical vapour deposition (PECVD), coupled with SiO_x interlayers from different growth techniques, were used to demonstrate the method. The experimental and simulation results confirm that the heavily doped poly-Si layer acts as the main gettering sink and the presence of different SiO_x interlayers determines the overall gettering rate. For the ultrathin SiO_x interlayers studied in this work, which have a similar thickness but different stoichiometry, a standard thermally grown SiO_x demonstrates the strongest blocking effect, followed by a chemically grown SiO_x from hot nitric acid, and a thermal SiO_x of a reduced stoichiometry (grown in a pure nitrogen ambient) demonstrates practically no blocking effect.

1. Introduction

Passivating contacts based on the structure of a heavily doped polysilicon layer on an ultrathin silicon oxide interlayer (poly-Si/SiO_x) have enabled substantial solar cell efficiency gains in recent years [1–3]. A wide range of techniques have been demonstrated to fabricate the poly-Si/SiO_x structure in a robust fashion (see, e.g., a review in Ref. [4]). These techniques, however, can result in very different impurity gettering effects during the structure formation process [5–9].

Due to cost constraints, solar-grade silicon materials are inherently less pure and the cleanliness of the photovoltaic manufacturing facilities is generally less well controlled than in the microelectronic industry. Removing impurities from the silicon wafer bulk to a region that has less of an adverse impact on the overall device performance, a process referred to as gettering, is therefore a crucial aspect of the solar cell fabrication process. Gettering of metallic impurities by the heavily

doped poly-Si/SiO_x during the high-temperature formation process was found to improve the bulk material quality of silicon substrates without compromising the surface passivation effect of poly-Si/SiO_x [5]. Understanding the gettering effects, kinetics and mechanisms of the poly-Si/SiO_x structures will enable further optimisation of the structure formation process to realise mass-production of high-efficiency solar cells on low-cost silicon materials.

In order to understand the different gettering effects of various poly-Si/SiO_x structures, this work aims to demonstrate a method to separate and quantify the individual impact of each component on the overall gettering effect of the poly-Si/SiO_x. These components include the heavily doped poly-Si layer, which acts as the main gettering sink [6]; the ultrathin SiO_x interlayer, which in some cases hinders the transport of impurities from the silicon wafer bulk to the poly-Si gettering layer [5]; and the heavily doped crystalline silicon (c-Si) near-surface region directly beneath the SiO_x interlayer, which may contribute to an

* Corresponding author.

E-mail address: Anyao.liu@anu.edu.au (A. Liu).

additional gettering effect because of heavy doping [10]. Combining the effect of each component, the overall gettering effect of the poly-Si/SiO_x structure during the applied formation process can then be reproduced.

2. Experimental details

A flowchart summary of the experimental procedures is shown in Fig. 1.

Iron (Fe) was used as a marker impurity in silicon to assess the gettering effect. High-quality float-zone (FZ) silicon wafers with intentional Fe contamination were prepared. The silicon wafers were boron doped with a bulk resistivity of 2.5 Ωcm, and were 290 ± 10 μm thick after surface etching in a tetramethylammonium hydroxide (TMAH) solution. Intentional Fe contamination into the silicon wafer bulk was achieved by ion implantation of ⁵⁶Fe and subsequent high-temperature (1000 °C) annealing to distribute Fe atoms evenly throughout the wafer thickness. The wafers were unloaded from furnace at a high temperature of 900 °C to minimise Fe precipitation, as the solubility limit of Fe at 900 °C [11] is above the implanted Fe concentrations of 10¹² – 10¹³ cm⁻³ (volumetric concentration after distribution) and a rapid cool-down in high air flow (within minutes) is highly unlikely to cause significant precipitation effects. The high-temperature distribution anneal was carried out in a dry oxygen and subsequently nitrogen ambient, which promoted the growth of surface silicon dioxide layers for surface passivation effects. This allowed minority carrier lifetime measurements to determine the dissolved interstitial Fe (Fe_i) concentrations in the silicon wafer bulk (technique to be detailed below). The bulk Fe_i concentrations were found to agree well with the implanted Fe doses, indicating minimal Fe precipitates in the samples. Further details of the ion implantation and annealing process can be found in Refs. [12,13].

Silicon wafers with no intentional Fe contamination were included as

control samples to monitor the surface passivation and process-induced Fe contamination levels in the silicon wafer bulk. The control samples consisted of both n-type ~100 Ωcm FZ and p-type 2.5 Ωcm FZ silicon wafers. The latter ones were the same as those used for Fe implantation, and were co-processed during the high-temperature distribution anneal.

Lifetime samples with symmetric poly-Si/SiO_x structures were then prepared. The thermally grown silicon dioxide layers were removed in a dilute hydrofluoric acid (HF) solution and the wafers were then cleaned in a standard Radio Corporation of America (RCA) cleaning process. After that, the silicon wafers underwent different SiO_x growth methods: chemically grown SiO_x in hot nitric acid, and thermally grown SiO_x at 600 °C with two different oxygen/nitrogen gas ratios, resulting in SiO_x layers of different stoichiometry [14]. One set of the thermal SiO_x layers was grown in a gas atmosphere containing oxygen and nitrogen, representing a standard thermal SiO_x interlayer, and its detailed characterisation can be found in Ref. [14] (denoted as “TO 1” in Ref. [14]). This SiO_x is referred to as “thermal SiO_x” in this paper. The other thermally grown SiO_x layers were grown in a pure nitrogen ambient, and are expected to be less stoichiometric than “TO 1” in Ref. [14]. This is denoted as “less stoichiometric thermal SiO_x” in this paper. The thicknesses of the nitric, thermal, and less stoichiometric thermal SiO_x layers were 1.3 nm, 1.2 nm, and 1.2 nm, respectively, from spectroscopic ellipsometry. One set of the samples had no SiO_x layer prior to the amorphous silicon (a-Si) deposition.

The samples were then coated with 40-nm phosphorus (P) in-situ doped a-Si films on both sides via plasma-enhanced chemical vapour deposition (PECVD), using a Centrotherm cPLASMA 2000 PECVD tool [15,16]. The film thickness was measured by spectroscopic ellipsometry. The samples then received high-temperature annealing to activate/-diffuse the dopants and recrystallise a-Si into poly-Si films. The annealing condition was 800 °C for 20 min in nitrogen, with a ramp-up from 750 °C at a rate of 10 °C/min and a ramp-down to 750 °C at a rate of 3 °C/min. A remote plasma hydrogenation process (RPHP) [17] at 400 °C for ~30 min was performed to further enhance the passivation quality of the poly-Si/SiO_x structures.

Cumulative anneals at fixed temperatures (650–900 °C) were planned after the poly-Si/SiO_x formation process (i.e. the aforementioned 800 °C activation and 400 °C hydrogenation). However, because the formation process itself was found to already getter a fraction of Fe from the silicon wafer bulk to the poly-Si layer, in some cases the remaining bulk Fe concentrations were too low to allow an accurate measurement of the subsequent bulk Fe loss kinetics during fixed-temperature anneals. Since the distribution of Fe in the poly-Si layer and the silicon wafer bulk depends on the segregation coefficient (k_{seg}) of the poly-Si at steady state and the k_{seg} decreases with increasing temperature (as will be shown later in Sect 4.2.1), annealing at a higher temperature (higher than the temperature of the last process step) drives some Fe from the poly-Si back into the silicon wafer bulk, thus increasing the initial bulk Fe concentrations prior to the fixed-temperature anneals. In other words, Fe can be cycled in different regions of the sample depending on the annealing temperature (i.e. the temperature-dependent k_{seg} , as will be shown in Eq (1) later).

Therefore, prior to each set of the cumulative anneals at 650 °C, 700 °C and 750 °C, the samples went through an 800 °C anneal from minutes to tens of minutes to drive a fraction of Fe back into the silicon wafer bulk. The exact amount of time needed to reach steady state depends on the blocking effects of the different SiO_x interlayers and was guided by the kinetic simulation (to be detailed below). 800 °C was chosen as it was found to have a minimal impact on the sheet resistance of the samples after annealing for a relatively short time, indicating insignificant dopant in-diffusion. The reverse process of Fe diffusing back into the silicon wafer bulk was also traced at 800 °C to study the kinetics. Since the gettering kinetics at 850 °C and 900 °C are too fast to be accurately measured, only the steady state conditions were measured and confirmed by additional anneals.

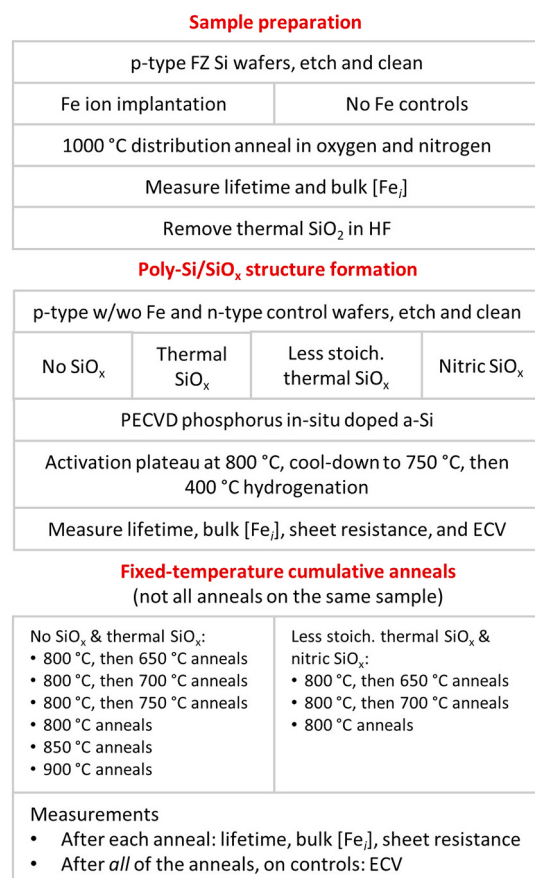


Fig. 1. A flowchart of the experimental procedures.

The fixed-temperature anneals were carried out in a nitrogen ambient. The samples were loaded in and out of the tube furnace at the respective annealing temperature, and were rapidly cooled down in a high air flow within minutes. The effective minority carrier lifetime, Fe_i concentration in the silicon wafer bulk, and sheet resistance of the samples were measured after each annealing step. The dopant depth profile was measured after contact formation and then after all of the annealing steps on control samples.

The effective minority carrier lifetime of the samples was measured by a photoconductance-based lifetime tester (WCT-120 from Sinton Instruments) [18], either in a quasi-steady-state or a transient decay mode. The sheet resistance of the samples was measured by both four-point-probe and dark conductance from the lifetime tester. The electrically active phosphorus depth profile was measured by electrochemical capacitance-voltage (ECV) using a WEP Wafer Profile CVP21 tool.

The Fe_i concentration in the bulk of p-type silicon wafers was measured by a lifetime-based technique, from comparing the effective minority carrier lifetimes before and after Fe-B pair dissociation via strong illumination [19–21]. This technique enables the effects of other light-insensitive recombination channels, such as surface recombination, to be “cancelled out” in the calculation of the bulk Fe_i concentrations. The surface lifetime (i.e. lifetime solely due to surface recombination) was estimated from the control samples with no intentional Fe contamination. The exact surface lifetime is in principle not critical, as long as the bulk lifetime due to Fe contamination is the dominating effect. This was mostly the case for the poly-Si/SiO_x samples. The samples without the SiO_x interlayer, however, had much poorer surface passivation such that the surface lifetimes and bulk Fe lifetimes were comparable on the same order of magnitude, especially after gettering. This led to much bigger uncertainties in the calculated bulk Fe concentrations in these no SiO_x samples, as will be shown later in the results. A 5% uncertainty in lifetime measurements [22] before and after Fe-B pair breaking was assumed to estimate the uncertainty in bulk Fe_i concentration.

3. Simulation details

As the heavily doped poly-Si layer was identified to be the main gettering region in the poly-Si/SiO_x structure [6] and gettering was found to occur through a segregation mechanism [5,6], the gettering kinetics are simulated based on a diffusion-limited segregation gettering model, using the algorithm outlined in Ref. [23] to numerically calculate Fe diffusion and segregation in the c-Si/SiO_x/poly-Si structure.

The diffusivity and solubility of Fe in the c-Si wafer bulk, denoted here as D_{c-Si}^{Fe} and S_{c-Si}^{Fe} , respectively, were from Refs. [11,24]. By the definition of the segregation coefficient (k_{seg}), the solubility of Fe in the poly-Si (S_{poly}^{Fe}) was determined from the k_{seg} of Fe from c-Si to poly-Si: $S_{poly}^{Fe} = S_{c-Si}^{Fe} \times k_{seg}$. The k_{seg} of Fe from c-Si to poly-Si was experimentally determined from the initial and final steady state Fe concentrations in the silicon wafer bulk, by the conservation of mass [25]:

$$k_{seg} = \frac{[Fe]_{poly_ss}}{[Fe]_{c-Si_ss}} = \frac{([Fe]_{c-Si_init} - [Fe]_{c-Si_ss}) \times t_{wafer} / t_{poly}}{[Fe]_{c-Si_ss}} \quad \text{Eq (1)}$$

where $[Fe]_{poly_ss}$ is the Fe concentration in the poly-Si layer at steady state, $[Fe]_{c-Si_init}$ and $[Fe]_{c-Si_ss}$ are the initial and steady state Fe concentrations in the c-Si wafer bulk, and t_{poly} and t_{wafer} are the thicknesses of the poly-Si layer and silicon wafer (half wafer thickness if gettering on both sides).

Note that Eq (1) assumes that all Fe atoms that are lost from the silicon wafer bulk are relocated to the poly-Si layer, which is valid if the total amount of Fe gettered by the other regions, the in-diffused surface region and the ultrathin SiO_x interlayer, is negligible in comparison. Otherwise, the Fe concentrations in these other layers need to be

accounted for in the conservation of mass. Eq (1) was used in most parts of this work, as will be explained later.

As will be shown later in Sect 4.2.2, the Fe concentration in the silicon wafer bulk reaches a steady state after a sufficiently long annealing time. At high temperatures of 800–900 °C, the steady state Fe concentrations are below the solid solubilities of Fe in c-Si [11,24], which again confirms the segregation gettering mechanism. Eq (1) assumes a constant k_{seg} in the poly-Si layer, which is reasonable here as the phosphorus concentration in the in-situ doped poly-Si layer is relatively uniform and does not change significantly during annealing (Sect 4.2.3).

The diffusivity of Fe in the heavily doped poly-Si is unknown, and is probably affected by the gettering (in other words, trapping) capacity of the poly-Si layer. Similar to the approach used in modelling phosphorus diffusion gettering (PDG) in c-Si [25], the Fe diffusivity in the poly-Si gettering layer (D_{poly}^{Fe}) was estimated by $D_{poly}^{Fe} = D_{c-Si}^{Fe} / k_{seg}$. Simulations showed that assuming $D_{poly}^{Fe} = D_{c-Si}^{Fe}$ produced the same result as $D_{poly}^{Fe} = D_{c-Si}^{Fe} / k_{seg}$, as was previously observed in modelling PDG [25], since the diffusion through the silicon wafer bulk remains as the rate-limiting factor for the gettering process (without considering the blocking effect of the SiO_x interlayer).

The diffusivity and solubility of Fe in different SiO_x layers (denoted as D_{ox}^{Fe} and S_{ox}^{Fe}) are even less certain and were treated as fitting parameters in the simulation. As summarised in Ref. [26], the data of D_{ox}^{Fe} in the literature are sparse, and there are conflicting S_{ox}^{Fe} data in the literature. The diffusion kinetics is determined by the flux, which is proportional to the product of diffusivity and solubility, as well as the difference in the supersaturation ratios of any two regions (defined as two nodes in numerical simulation) [23]. The difference in the supersaturation ratios, or the difference in the concentrations if both nodes are within the same material, diminishes as the segregation process approaches steady state. Therefore, to quantify the diffusion process, in this work we will report the fitted product of diffusivity and solubility, $D_{ox}^{Fe}S_{ox}^{Fe}$, in different SiO_x interlayers. For the same $D_{ox}^{Fe}S_{ox}^{Fe}$, different combinations of D_{ox}^{Fe} and S_{ox}^{Fe} produce the same kinetics, unless S_{ox}^{Fe} is so high (e.g. higher than S_{poly}^{Fe}) such that Eq (1) needs to be modified to account for a high Fe concentration in the ultrathin SiO_x interlayer.

Lastly, the simulated Fe concentration profiles (depth-wise in the c-Si/SiO_x/poly-Si structure) were averaged to produce the average Fe concentration in the silicon wafer bulk, as a function of annealing time, in order to compare with the experimentally measured Fe reduction kinetics. Before gettering steady state is reached, the Fe distribution across the wafer thickness is non-uniform as gettering sinks are only present on the wafer surfaces. Nevertheless, the measurement of average Fe concentrations from the lifetime-based Fe-B pair dissociation technique was found to be not significantly affected by the inhomogeneous Fe distribution across the wafer thickness [27].

4. Results and discussion

4.1. Comparison after a typical formation process

Fig. 2 compares the fraction of the remaining Fe concentration in the silicon wafer bulk after a typical poly-Si/SiO_x structure formation process (high-temperature anneal and hydrogenation), for samples with no or different SiO_x interlayers. Despite the different SiO_x interlayers, all of the poly-Si/SiO_x samples obtained a good surface passivation effect, with the implied V_{oc} of the p-type control samples in the range of 710–725 mV, representing a typical cell process (i.e. process not optimised for gettering). On the other hand, the p-type no SiO_x samples had a low implied V_{oc} of 615 mV, as expected. The process-induced bulk Fe contamination was estimated to be on the order of 10^9 cm^{-3} , which is well below the remaining Fe concentrations in the intentionally-contaminated samples (on the order of $10^{11} – 10^{12} \text{ cm}^{-3}$). Because the samples had different initial bulk Fe concentrations in the range of

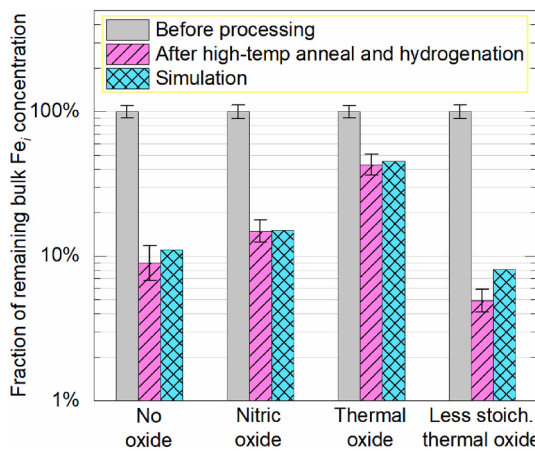


Fig. 2. Experimental and simulated fraction of the remaining Fe concentration in the silicon wafer bulk after high-temperature activation (800 °C) and hydrogenation (400 °C). The samples had the same PECVD phosphorus-doped poly-Si layers but different SiO_x interlayers. (For interpretation of the references to colour in this figure legend, the reader is referred to the Web version of this article.)

10¹² – 10¹³ cm⁻³, the remaining Fe concentrations were normalised to the respective initial concentrations. That is, the 100% mark in Fig. 2 indicates the initial bulk Fe concentration from ion implantation prior to any gettering process.

As the samples had the same poly-Si layers (the predominant gettering sink [6]) and the different SiO_x interlayers only affect the gettering rates but not the gettering capacity of the poly-Si layers (to be shown later), the different fractions shown in Fig. 2 reflect the different blocking effects of the SiO_x interlayers.

The sample with no SiO_x interlayer had no such blocking effect, and its result reveals the full gettering potential of this particular poly-Si film during this particular temperature-time profile. As will be shown later in Sect 4.2.3, dopant in-diffusion into the c-Si wafer bulk after structure formation (without further anneals) had only a small impact on the overall gettering effect, even for the no SiO_x samples. The results in Fig. 2 indicate that, the standard thermal SiO_x has the largest blocking effect, followed by the chemically grown nitric SiO_x and then the less stoichiometric thermal SiO_x, which practically has no blocking effect. The slightly lower bulk Fe concentration in the less stoichiometric thermal SiO_x sample compared to the no SiO_x sample is partly due to a small difference in wafer thicknesses, as the simulated (i.e. expected) residual Fe concentration ratios are 8% for the less stoichiometric thermal SiO_x sample (slightly thinner) and 11% for the no SiO_x sample. However, it is yet unclear what caused the additional reduction in the Fe concentration ratio in this less stoichiometric thermal SiO_x sample.

Combining the effect of each component (poly-Si, SiO_x interlayer, and heavily doped c-Si surface region), as will be characterised in the following sections, the overall gettering kinetics of the poly-Si/SiO_x structure can be simulated. The resulting bulk Fe concentrations are simulated considering the whole applied formation process, which involved an 800 °C 20 min anneal with a 3 °C/min ramp-down to 750 °C and a subsequent 400 °C 30 min hydrogenation step. As shown in Fig. 2, a generally good agreement with the experimental results is evident.

4.2. Quantifying the impact of each component

To unravel the individual impacts of the heavily doped poly-Si layer and SiO_x interlayer, fixed-temperature anneals were carried out to study the temperature-dependent gettering kinetics. After a sufficiently long annealing time, the residual Fe concentrations in the silicon wafer bulk reach a steady state level, and as shown in Eq (1) this steady state Fe concentration ratio reflects the gettering strength of the poly-Si layers

(Sect 4.2.1). The gettering kinetics (in other words, gettering rate) depends on the blocking effect of the SiO_x interlayer. By fitting the experimental gettering kinetics, the transport of Fe through different SiO_x interlayers can be quantified (Sect 4.2.2). Lastly, the gettering effect of the in-diffused c-Si surface regions can be estimated from the depth profiles of the electrically active phosphorus concentration (Sect 4.2.3).

4.2.1. Gettering strength of the poly-Si layer

The segregation gettering strength is commonly quantified by the segregation coefficient, k_{seg} , which is the ratio of the impurity solubility in the gettering region (in this case, heavily doped poly-Si) to the solubility in the performance-affected region (in this case, c-Si wafer bulk). As shown in Eq (1), k_{seg} can be estimated from the initial and final steady state Fe concentrations in the silicon wafer bulk, which can be experimentally determined from the fixed-temperature anneals.

Fig. 3 compiles the experimentally measured k_{seg} of all of the samples, regardless of the presence or type of the SiO_x interlayer, at a range of annealing temperatures. As will be shown later in Sect 4.2.2, the presence of different SiO_x interlayers only affects the gettering rate, but not the gettering strength (i.e. k_{seg}) of the poly-Si layer. In addition, although different degrees of dopant in-diffusion are expected for samples with no or different SiO_x interlayers, the in-diffused amount is too small to significantly affect the high doping concentration in the poly-Si layer (Sect 4.2.3).

From the temperature-dependent k_{seg} data, the activation energy (E_a) of this segregation gettering process for Fe is estimated to be 2.4 ± 0.2 eV (or more precisely, -2.4 ± 0.2 eV, as the reaction is exothermic). E_a indicates the enthalpy change between the gettered and un-gettered states [10].

As the gettering effect of intrinsic poly-Si is weak and gettering is mainly caused by a high dopant concentration [5], we compare the k_{seg} of P-doped poly-Si to the k_{seg} of P-doped c-Si from the literature. The literature k_{seg} values were extracted from semi-empirical models assuming a pairing reaction between substitutional P and interstitial Fe, with the assistance of vacancies [25,28–30]. The electrically active substitutional P concentration ([P⁺]) in the poly-Si layers was measured by ECV and is around 7 × 10¹⁹ cm⁻³ (see Sect 4.2.3). This [P⁺] was used to compute the literature k_{seg} values in Fig. 3.

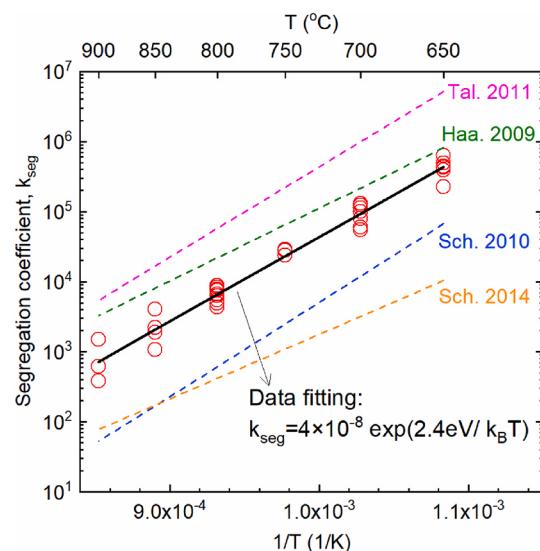


Fig. 3. Temperature-dependent segregation coefficients of the PECVD in-situ P-doped polysilicon layer used in this work (symbols). Also included in this figure are the segregation coefficients from phosphorus diffusion gettering in c-Si assuming Fe pairing with electrically active P dopants, from Haarahiltunen et al. [25], Talvitie et al. [28], and Schön et al. [29,30].

As shown in Fig. 3, the literature k_{seg} of the heavily P-doped c-Si can vary by 2–3 orders of magnitude and our experimental data lie somewhere in between. The large variation in the reported k_{seg} values highlights the uncertainties associated with quantifying phosphorus diffusion gettering, as there are multiple models proposed in the literature to explain the gettering mechanisms (e.g. see a brief discussion in Ref. [30]). In addition, although the measured $[P^+]$ in the poly-Si layers is well below the solubility limit of P in Si [31], we cannot rule out the possible presence of electrically inactive P in the poly-Si, which can contribute to additional gettering effects [32,33]. Furthermore, our test conditions, in terms of $[P^+]$ and temperatures, may not fully fall within the experimental ranges examined in Refs. [25,28–30]. Nonetheless, the comparison in Fig. 3 gives us confidence in our experimental k_{seg} values of the heavily P-doped poly-Si. The gettering strength of the heavily P-doped poly-Si seems to be comparable with the phosphorus diffusion in c-Si of the same doping concentration.

4.2.2. Blocking effect of the SiO_x interlayer

It was previously observed that the presence of SiO_x interlayers adversely affects the gettering effect of poly-Si/ SiO_x after a typical formation process, which was speculated to be due to a reduced mobility of impurities through the SiO_x interlayer [5]. To examine this hypothesis and to quantify the Fe transport in SiO_x , simulations were carried out to model the diffusion-limited segregation gettering kinetics and fit the experimental data.

i). Simulation verification

As detailed in Sect 3, the only fitting parameter in the simulation is the product of Fe diffusivity and solubility in SiO_x , $D_{\text{ox}}^{\text{Fe}}S_{\text{ox}}^{\text{Fe}}$. For the samples with no SiO_x interlayer, there is no fitting parameter in the simulation. The good agreement between simulation and experiment for the no SiO_x samples (see Fig. 4) verifies the simulation approach. In addition, samples with different initial bulk Fe concentrations demonstrate similar gettering kinetics and segregation coefficients, which again confirms segregation as the main gettering mechanism.

The injection of hydrogen into the silicon wafer bulk was conjectured to affect the diffusivity of Fe in silicon [34]. As the no SiO_x samples exhibit gettering kinetics that can be well described by the literature reported Fe diffusivity in silicon, a modified Fe diffusivity due to possible bulk hydrogenation effects, such as from the applied RPHP, is not observed in this work. Moreover, samples prepared with or without a prior RPHP demonstrate similar gettering kinetics (to be published), indicating a negligible impact of bulk hydrogenation on the measured Fe gettering kinetics.

As mentioned previously, due to the poor surface passivation of the samples without a SiO_x interlayer, the error bars in the measured bulk Fe concentrations are very large, especially at low Fe concentration levels (Fig. 4). Some of the lower error bars even extend to zero Fe concentrations, such as the ones in Fig. 4(a) where the lower error bars are not fully displayed. Nevertheless, the consistency of the steady state data suggests a likely overestimation of the uncertainty range in these no SiO_x samples.

ii). Simulating the reverse process

Intuitively, a gettering process reduces the impurity concentration in the silicon wafer bulk. However, as the gettering strength decreases with increasing temperature (Fig. 3), annealing at a higher temperature triggers a re-distribution of impurities that results in an increased bulk impurity concentration. An example is shown in Fig. 5, where the sample was previously annealed at 650 °C to steady state and was then subjected to 800 °C anneals. Since the model only depends on the segregation coefficient and diffusion parameters, the kinetics of the reverse process (i.e. Fe diffusion from poly-Si to c-Si through a SiO_x interlayer) can also be simulated, as demonstrated in Fig. 5.

iii). Comparing the blocking effects of different SiO_x interlayers

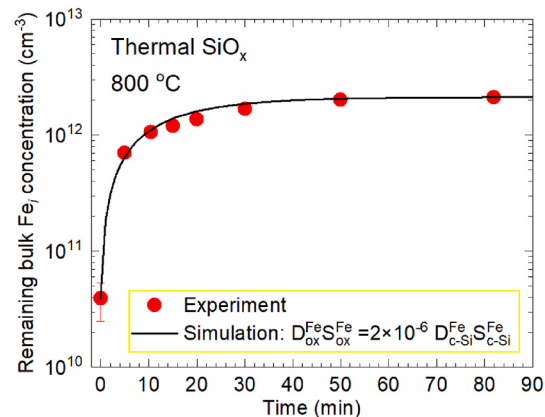


Fig. 5. Gettering kinetics at 800 °C, for a thermal SiO_x sample. Prior to the 800 °C anneals, the sample reached the gettering steady state at 650 °C, and thus a lower initial Fe concentration in the silicon wafer bulk than the steady state at 800 °C. (For interpretation of the references to colour in this figure legend, the reader is referred to the Web version of this article.)

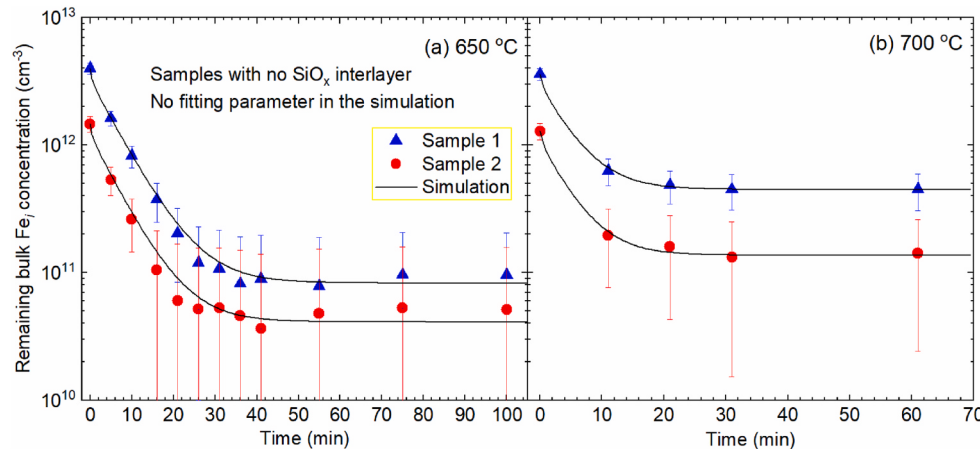


Fig. 4. Gettering kinetics of the samples with no SiO_x interlayer, at annealing temperatures of (a) 650 °C and (b) 700 °C. Symbols are experimental data and lines are simulation results.

Fig. 6 presents a comparison of the gettering kinetics at 700 °C for samples with no or different SiO_x interlayers. The 100% mark in **Fig. 6** indicates the initial bulk Fe concentrations prior to this set of cumulative anneals at 700 °C (see experiment flowchart in **Fig. 1**). As shown in **Fig. 6**, although there are variations in the final steady state fractions of the remaining bulk Fe concentrations (note the logarithmic scale), the difference is within a factor of two, which is quite small compared to the variations as a function of temperature (see **Fig. 3**). This small difference in the steady state Fe concentration ratios is possibly due to slight uniformity issues in PECVD. The presence of different SiO_x interlayers is shown to only change the gettering rate, but not the final steady state fraction of the remaining bulk Fe concentrations. The same was also observed from comparing the gettering kinetics at 650 °C (data not shown).

The different gettering kinetics of the samples with different SiO_x interlayers can be well described by simulations assuming different $D_{ox}^{Fe}S_{ox}^{Fe}$ in SiO_x. The less stoichiometric thermal SiO_x and one of the nitric SiO_x samples (labelled as “Nitric SiO_x, 1”) exhibit the same gettering rate as the no SiO_x samples, and therefore the fitted $D_{ox}^{Fe}S_{ox}^{Fe}$ in SiO_x is the same as in c-Si: $D_{ox}^{Fe}S_{ox}^{Fe} = D_{c-Si}^{Fe}S_{c-Si}^{Fe}$. Due to the limited sensitivity of the average bulk Fe concentration to a high Fe transport through an ultrathin SiO_x interlayer, $D_{ox}^{Fe}S_{ox}^{Fe} = 5 \times 10^{-4} D_{c-Si}^{Fe}S_{c-Si}^{Fe}$ can also fit the experimental data, providing a lower bound for the $D_{ox}^{Fe}S_{ox}^{Fe}$ in such SiO_x layers. Nevertheless, from a practical point of view, these SiO_x interlayers have no blocking effect.

One of the nitric SiO_x samples (labelled as “Nitric SiO_x, 2”) shows a slower gettering kinetics that can be simulated by assuming $D_{ox}^{Fe}S_{ox}^{Fe} = 1.5 \times 10^{-5} D_{c-Si}^{Fe}S_{c-Si}^{Fe}$. There were 2–3 Fe-contaminated samples per test condition, and only the nitric SiO_x samples demonstrate such sample-to-sample variations in the gettering kinetics, which may be caused by a non-uniform growth of the chemical SiO_x layers in hot nitric acid.

Standard thermal SiO_x interlayers illustrate the strongest blocking effect, which can be fitted by a much reduced Fe transport in SiO_x: $D_{ox}^{Fe}S_{ox}^{Fe} = 2 \times 10^{-6} D_{c-Si}^{Fe}S_{c-Si}^{Fe}$.

Also shown in **Fig. 6** are the simulated gettering kinetics using D_{ox}^{Fe} from the literature [26] and assuming different S_{ox}^{Fe} scenarios. As discussed in Ref. [26], the solubility data of Fe in SiO_x varies by such a large extent that there is no consensus on whether the solubility in SiO_x is higher or lower than that in c-Si, and experimental evidence for both cases are available in the literature. We also observed experimentally either no Fe segregation into thick (tens of nm) thermal SiO_x surface layers from secondary ion mass spectrometry (SIMS) [13,35], or a seemingly comparable Fe concentration in nitric SiO_x and in heavily doped poly-Si in a poly-Si/SiO_x/c-Si structure from atom probe tomography (publication under preparation [36]). It is suspected that the different Fe solubilities may be caused by different SiO_x properties.

As shown in **Fig. 6**, the combination of literature D_{ox}^{Fe} and $S_{ox}^{Fe} = S_{c-Si}^{Fe}$ produces a gettering kinetics that would take years to happen, which

certainly disagrees with the experimental findings here and elsewhere [5–9]. Assuming the same Fe solubility in SiO_x and in heavily doped poly-Si, that is, a strong segregation of Fe into SiO_x, yields a gettering kinetics that are closer to the experimental data of the thermal SiO_x samples, although still slower. However, it is worth emphasising that this comparison does not indicate that Fe strongly segregates to the SiO_x interlayers, as the actual Fe diffusivities in ultrathin SiO_x interlayers may deviate significantly to the literature D_{ox}^{Fe} values, which were derived from very thick (hundreds of nm) silicon oxide layers.

The analysis of the fixed-temperature gettering kinetics was extended to several temperatures and the resulting fitted $D_{ox}^{Fe}S_{ox}^{Fe}$ are plotted in **Fig. 7**, along with the literature values. For the investigated temperature range of 650–800 °C, the SiO_x blocking effect is shown to increase from the less stoichiometric thermal SiO_x (practically no blocking effect), to the nitric SiO_x in some cases, and then to the standard thermal SiO_x interlayers which demonstrate the strongest blocking strength. These findings from the fixed-temperature anneals are consistent with the experimental results from a typical contact

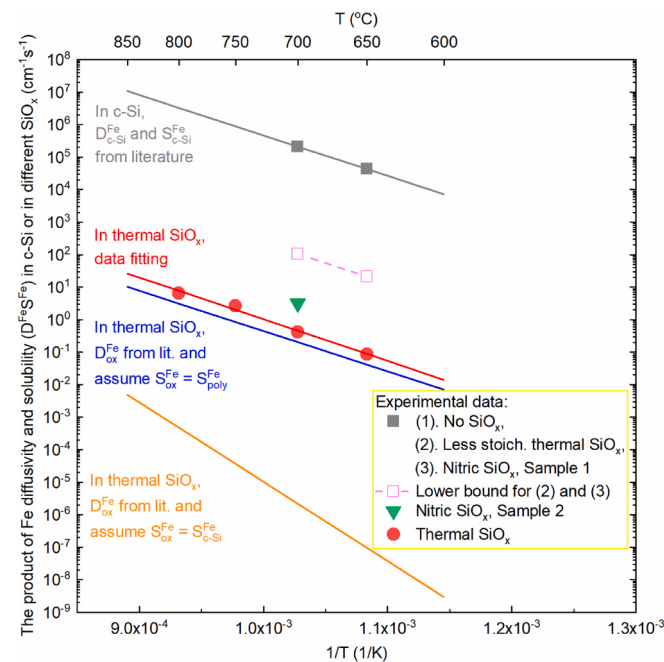


Fig. 7. Comparison of the product of Fe diffusivity and solubility in c-Si and in different SiO_x interlayers. Symbols are from fitting experimental gettering kinetics, and lines are either calculations based on the literature Fe diffusivity and solubility [11,24,26], or from data fitting the experimentally extracted $D_{ox}^{Fe}S_{ox}^{Fe}$ values.

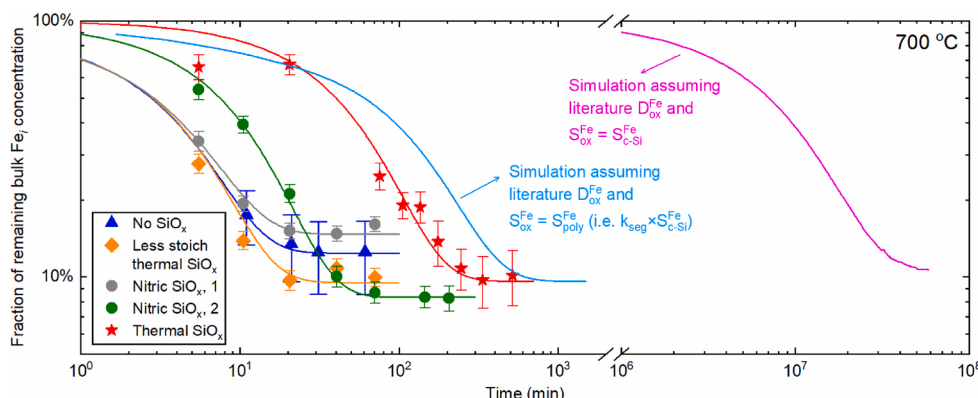


Fig. 6. Experimental (symbols) and simulated (lines) gettering kinetics at 700 °C, for samples with no or different SiO_x interlayers and with the same PECVD P-doped poly-Si films. The literature diffusivity of Fe in silicon oxide is from Istratov et al. [26]. The nitric SiO_x samples show different gettering kinetics and therefore both are included in the plot, labelled as “Nitric SiO_x, 1” and “Nitric SiO_x, 2”. The samples with other types of SiO_x interlayers, or no SiO_x, demonstrate consistent gettering kinetics and thus only one set of data is shown here. (For interpretation of the references to colour in this figure legend, the reader is referred to the Web version of this article.)

formation process (Sect 4.1).

4.2.3. Gettering effect of the in-diffused c-Si surface region

To assess the contribution from the in-diffused c-Si surface region on the overall gettering effect, the electrically active P dopant concentration, $[P^+]$, in the poly-Si/SiO_x/c-Si samples was measured by ECV. Fig. 8 shows the $[P^+]$ profiles first after the structure formation process, and then at the end of all of the further fixed-temperature annealing steps (see the experiment flowchart in Fig. 1). As can be seen in Fig. 8, dopant in-diffusion into c-Si is not significant, except for the samples with no SiO_x interlayer especially after further high temperature anneals, as expected.

The amount of Fe that is gettered by the heavily doped c-Si surface region can be estimated from the reported segregation coefficient of P-doped c-Si for Fe [25,28–30]. As previously shown in Fig. 3, there is a large variation in the reported k_{seg} values. Here we used the k_{seg} models from Haarahlitunen et al. [25] and Schön et al. [29] to evaluate the upper and lower bounds of the gettered Fe concentrations, respectively, as these two are closer to our own experimental data (Fig. 3).

Due to the limited depth resolution of ECV, the 1.3-nm SiO_x interlayer and the onset of the c-Si wafer bulk cannot be exactly located on the ECV profiles. However, it is reasonable to assume that the interface is where the $[P^+]$ profile starts to drop. This may slightly overestimate the gettered Fe concentration in the in-diffused c-Si region.

The ECV etch depths of the poly-Si layers are consistently observed to be smaller than the thicknesses measured by spectroscopic ellipsometry (unpublished results). This is likely caused by an underestimated etch rate of the poly-Si in ECV, as briefly commented on in Ref. [37]. The depth measurement of the c-Si region, however, is well calibrated and thus does not affect the estimation of the gettering effect of the in-diffused c-Si region.

For the nitric, thermal, and less stoichiometric thermal SiO_x samples after further fixed-temperature anneals, which have similar ECV profiles (comparison not shown here), the fraction of Fe that is gettered by the in-diffused region to the total Fe concentration in the whole poly-Si/SiO_x/c-Si system is in the range of 0.1%–5% at 650–800 °C, calculated from Refs. [25,29]. The fraction is the same for the no SiO_x samples just after structure formation. After further high temperature annealing, the fraction for the no SiO_x samples changes to 0.5%–16% due to stronger dopant in-diffusion. Therefore, the results confirm that the majority of the Fe is gettered by the heavily doped poly-Si layer in this work.

5. Conclusion

To understand the gettering effects of various poly-Si/SiO_x passivating contact structures, we have presented a method to separate and

quantify the individual impact of each component on the overall gettering effectiveness. These components are identified to be, i) the heavily doped poly-Si layer, which serves as the predominant gettering region; ii) the SiO_x interlayer, which is a diffusion barrier that determines the overall gettering rate; and iii) the in-diffused c-Si surface region, which may contribute to an additional gettering effect depending on the doping level.

The gettering capacity of the poly-Si layer is quantified by a temperature-dependent segregation coefficient, from the initial and final steady state Fe concentrations in the silicon wafer bulk. The diffusion parameter (the product of Fe diffusivity and solubility) associated with the SiO_x interlayer is extracted via fitting the experimental gettering kinetics by a numerical simulation of the diffusion-limited segregation gettering process. The gettering effect of the in-diffused c-Si surface region is estimated from the dopant depth profile and the reported segregation coefficient of the heavily doped c-Si.

The experimental results and simulation confirm that the heavily doped poly-Si layer is the main gettering sink, and the blocking effect of the SiO_x interlayers only slows down the gettering rate, but does not affect the gettering strength of the heavily doped poly-Si layer, as long as there is no strong dopant in-diffusion to significantly alter the doping level in the poly-Si layer. For the investigated SiO_x interlayers, which are of similar thickness but with different stoichiometry, the blocking effect is shown to increase from a less stoichiometric thermally grown SiO_x, which practically has no blocking effect, to a chemically grown nitric SiO_x, and then to a standard thermal SiO_x. That is, the gettering kinetics is slowest for the samples with thermal SiO_x interlayers. Nevertheless, if given sufficient time to allow impurity diffusion through the SiO_x interlayers, the full gettering potential of the poly-Si layer can be achieved.

Combining the temperature-dependent gettering effect of each component, the overall gettering effect of the poly-Si/SiO_x structure during a typical formation process can be simulated, and is shown to agree with experimental results. This provides a useful approach to enable future predictive modelling and optimisation of the gettering effectiveness in poly-Si/SiO_x cell fabrications.

CRediT authorship contribution statement

AnYao Liu: Conceptualization, Resources, Software, Investigation, Formal analysis, Visualization, Writing – original draft, Funding acquisition. **Zhongshu Yang:** Software, Investigation, Writing – review & editing. **Frank Feldmann:** Resources, Formal analysis, Writing – review & editing. **Jana-Isabelle Polzin:** Resources. **Bernd Steinhauser:** Resources. **Sieu Pheng Phang:** Software, Formal analysis, Writing – review & editing. **Daniel Macdonald:** Formal analysis, Writing – review & editing, Funding acquisition.

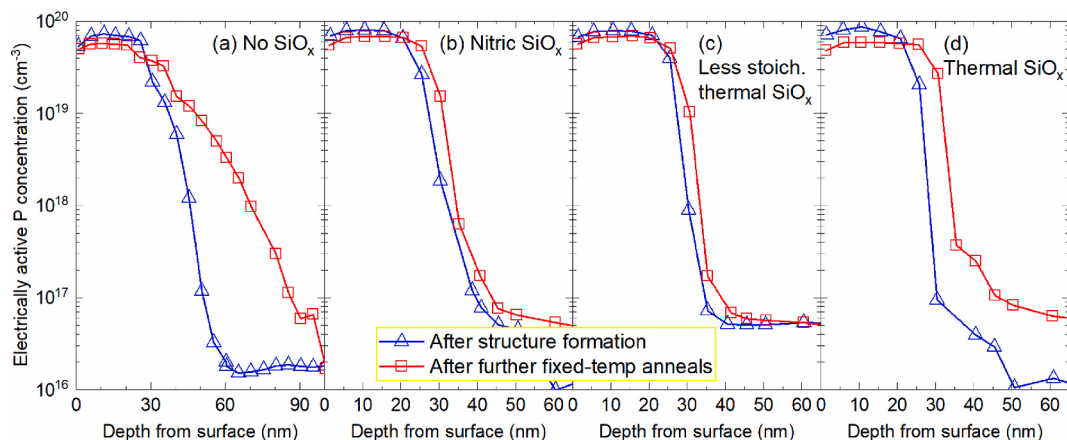


Fig. 8. ECV measurements of the electrically active phosphorus dopant concentration depth profiles in the samples without SiO_x or with different SiO_x interlayers, after a typical structure formation process (800 °C activation followed by 400 °C hydrogenation), and then after all of the cumulative annealing experiments.

Declaration of competing interest

The authors declare that they have no known competing financial interests or personal relationships that could have appeared to influence the work reported in this paper.

Acknowledgement

This work was supported by the Australian Renewable Energy Agency (ARENA) through project RND017 and the Australian Centre for Advanced Photovoltaics (ACAP). A. Liu acknowledges funding from the ACAP postdoctoral fellowship scheme. This work has been made possible through the access to the ACT node of the Australian National Fabrication Facility (ANFF-ACT).

References

- [1] F. Feldmann, M. Bivour, C. Reichel, M. Hermle, S.W. Glunz, Passivated rear contacts for high-efficiency n-type Si solar cells providing high interface passivation quality and excellent transport characteristics, *Sol. Energy Mater. Sol. Cell.* 120 (2014) 270–274.
- [2] S. Glunz, et al., The irresistible charm of a simple current flow pattern—25% with a solar cell featuring a full-area back contact, in: Proceedings of the 31st European Photovoltaic Solar Energy Conference and Exhibition, 2015, pp. 259–263.
- [3] F. Haase, et al., Laser contact openings for local poly-Si-metal contacts enabling 26.1%-efficient POLO-IBC solar cells, *Sol. Energy Mater. Sol. Cell.* 186 (2018) 184–193.
- [4] J. Schmidt, R. Peibst, R. Brendel, Surface passivation of crystalline silicon solar cells: present and future, *Sol. Energy Mater. Sol. Cell.* 187 (2018) 39–54.
- [5] A. Liu, D. Yan, S.P. Phang, A. Cuevas, D. Macdonald, Effective impurity gettering by phosphorus- and boron-diffused polysilicon passivating contacts for silicon solar cells, *Sol. Energy Mater. Sol. Cell.* 179 (2018) 136–141.
- [6] A. Liu, et al., Direct observation of the impurity gettering layers in polysilicon-based passivating contacts for silicon solar cells, *ACS Appl. Energy Mater.* 1 (5) (2018) 2275–2282.
- [7] J. Krügener, F. Haase, M. Rienäcker, R. Brendel, H.J. Osten, R. Peibst, Improvement of the SRH bulk lifetime upon formation of n-type POLO junctions for 25% efficient Si solar cells, *Sol. Energy Mater. Sol. Cell.* 173 (2017) 85–91.
- [8] M. Hayes, et al., Impurity gettering by boron- and phosphorus-doped polysilicon passivating contacts for high-efficiency multicrystalline silicon solar cells, *Phys. Status Solidi* 216 (17) (2019) 1900321.
- [9] Z. Wang, et al., Effective gettering of in-situ phosphorus-doped polysilicon passivating contact prepared using plasma-enhanced chemical-vapor deposition technique, *Sol. Energy Mater. Sol. Cell.* 206 (2020) 110256.
- [10] S.M. Myers, M. Seibt, W. Schröter, Mechanisms of transition-metal gettering in silicon, *J. Appl. Phys.* 88 (7) (2000) 3795–3819.
- [11] A.A. Istratov, H. Hieslmair, E.R. Weber, Iron and its complexes in silicon, *Appl. Phys. A* 69 (1999) 13–44.
- [12] D. Macdonald, P.N.K. Deenapanray, S. Diez, Onset of implant-related recombination in self-ion implanted and annealed crystalline silicon, *J. Appl. Phys.* 96 (7) (2004) 3687–3691.
- [13] A.Y. Liu, C. Sun, V.P. Markevich, A.R. Peaker, J.D. Murphy, D. Macdonald, Gettering of interstitial iron in silicon by plasma-enhanced chemical vapour deposited silicon nitride films, *J. Appl. Phys.* 120 (19) (2016) 193103.
- [14] J.-I. Polzin, et al., Temperature-induced stoichiometric changes in thermally grown interfacial oxide in tunnel-oxide passivating contacts, *Sol. Energy Mater. Sol. Cell.* 218 (2020) 110713.
- [15] B. Steinhauser, J.-I. Polzin, F. Feldmann, M. Hermle, S.W. Glunz, Excellent surface passivation quality on crystalline silicon using industrial-scale direct-plasma TOPCon deposition technology, *Solar RRL* 2 (7) (2018) 1800068.
- [16] F. Feldmann, et al., Large area TOPCon cells realized by a PECVD tube process, in: Proceedings of the 36th European Photovoltaic Solar Energy Conference and Exhibition, 2019, pp. 304–308.
- [17] S. Lindekugel, H. Lautenschlager, T. Ruof, S. Reber, Plasma hydrogen passivation for crystalline silicon thin-films, in: Proceedings of the 23rd European Photovoltaic Solar Energy Conference, 2008, pp. 2232–2235.
- [18] R.A. Sinton, A. Cuevas, Contactless determination of current-voltage characteristics and minority-carrier lifetimes in semiconductors from quasi-steady-state photoconductance data, *Appl. Phys. Lett.* 69 (17) (1996) 2510–2512.
- [19] G. Zoth, W. Bergholz, A fast, preparation-free method to detect iron in silicon, *J. Appl. Phys.* 67 (11) (1990) 6764–6771.
- [20] D.H. Macdonald, L.J. Geerligs, A. Azzizi, Iron detection in crystalline silicon by carrier lifetime measurements for arbitrary injection and doping, *J. Appl. Phys.* 95 (3) (2004) 1021–1028.
- [21] L. Geerligs, D. Macdonald, Dynamics of light-induced FeB pair dissociation in crystalline silicon, *Appl. Phys. Lett.* 85 (2004) 5227.
- [22] A.L. Blum, et al., Interlaboratory study of eddy-current measurement of excess-carrier recombination lifetime, *IEEE Journal of Photovoltaics* 4 (1) (2014) 525–531.
- [23] H. Hieslmair, S. Balasubramanian, A.A. Istratov, E.R. Weber, Gettering simulator: physical basis and algorithm, *Semicond. Sci. Technol.* 16 (2001) 567–574.
- [24] J.D. Murphy, R.J. Falster, Contamination of silicon by iron at temperatures below 800 °C, *Phys. Status Solidi RRL* 5 (2011) 370–372.
- [25] A. Haarahiltunen, H. Savin, M. Yli-Koski, H. Talvitie, J. Sinkkonen, Modeling phosphorus diffusion gettering of iron in single crystal silicon, *J. Appl. Phys.* 105 (2) (2009), 023510.
- [26] A.A. Istratov, H. Väinölä, W. Huber, E.R. Weber, Gettering in silicon-on-insulator wafers: experimental studies and modelling, *Semicond. Sci. Technol.* 20 (6) (2005) 568.
- [27] K. McLean, C. Morrow, D. Macdonald, Activation energy for the hydrogenation of iron in P-type crystalline silicon wafers, in: IEEE 4th World Conference on Photovoltaic Energy Conference, 7–12 May 2006 2006, vol. 1, 2006, pp. 1122–1125.
- [28] H. Talvitie, V. Vähäniemi, A. Haarahiltunen, M. Yli-Koski, H. Savin, Phosphorus and boron diffusion gettering of iron in monocrystalline silicon, *J. Appl. Phys.* 109 (9) (2011), 093505.
- [29] J. Schön, M.C. Schubert, W. Warta, H. Savin, A. Haarahiltunen, Analysis of simultaneous boron and phosphorus diffusion gettering in silicon, *Phys. Status Solidi* 207 (11) (2010) 2589–2592.
- [30] J. Schön, V. Vähäniemi, A. Haarahiltunen, M.C. Schubert, W. Warta, H. Savin, Main defect reactions behind phosphorus diffusion gettering of iron, *J. Appl. Phys.* 116 (24) (2014) 244503.
- [31] S. Solmi, A. Parisini, R. Angelucci, A. Armigliato, D. Nobili, L. Moro, Dopant and carrier concentration in Si in equilibrium with monoclinic SiP precipitates, *Phys. Rev. B* 53 (12) (1996) 7836–7841.
- [32] A. Ourmazd, W. Schröter, Phosphorus gettering and intrinsic gettering of nickel in silicon, *Appl. Phys. Lett.* 45 (7) (1984) 781–783.
- [33] R. Chen, B. Trzynadlowski, S.T. Dunham, Phosphorus vacancy cluster model for phosphorus diffusion gettering of metals in Si, *J. Appl. Phys.* 115 (5) (2014), 054906.
- [34] P. Karzel, A. Frey, S. Fritz, G. Hahn, Influence of hydrogen on interstitial iron concentration in multicrystalline silicon during annealing steps, *J. Appl. Phys.* 113 (11) (2013) 114903.
- [35] A.Y. Liu, D. Macdonald, Impurity gettering effect of atomic layer deposited aluminium oxide films on silicon wafers, *Appl. Phys. Lett.* 110 (19) (2017) 191604.
- [36] Yadav, Apurva; Nomoto, Keita; Yan, Di; Breen, Andrew; Yang, Wenjie; Liu, AnYao; Macdonald, Daniel; Ringer, Simon, "New insight into passivation and gettering in polysilicon passivating contacts to engineering higher efficiency solar cells," Under preparation.
- [37] F. Feldmann, M. Nicolai, R. Müller, C. Reichel, M. Hermle, Optical and electrical characterization of poly-Si/SiO_x contacts and their implications on solar cell design, *Energy Procedia* 124 (2017) 31–37.